PHYSICAL REVIEW D **92**, 123004 (2015)

CMB spectral distortions from the decay of causally generated magnetic fields

Jacques M. Wagstaff[1,2,*] and Robi Banerjee[1,2]

[1]*Hamburger Sternwarte, Gojenbergsweg 112, 21029 Hamburg, Germany*
[2]*Nordita KTH Royal Institute of Technology and Stockholm University Roslagstullsbacken 23, SE-106 91 Stockholm, Sweden*

(Received 28 July 2015; published 14 December 2015)

We improve previous calculations of the cosmic microwave background spectral distortions due to the decay of primordial magnetic fields. We focus our studies on causally generated magnetic fields at the electroweak and QCD phase transitions. We also consider the decay of helical magnetic fields. We show that the decay of nonhelical magnetic fields generated at either the electroweak or QCD scale produce μ- and y-type distortions below 10^{-8} which are probably not detectable by a future PIXIE-like experiment. We show that magnetic fields generated at the electroweak scale must have a helicity fraction $f_* > 10^{-4}$ in order to produce detectable μ-type distortions. Hence, a positive detection coming from the decay of magnetic fields would rule out nonhelical primordial magnetic fields and provide a lower bound on the magnetic helicity.

DOI: 10.1103/PhysRevD.92.123004 PACS numbers: 98.62.En, 95.30.Qd, 98.70.Vc, 98.80.Cq

I. INTRODUCTION

Magnetic fields are observed throughout the cosmos; from galaxies at high and low redshifts [1–3], in galaxy (super)clusters [4,5], and in the voids of the large scale structure [6]. Although still under debate, the difficulties of astrophysical mechanisms in explaining such observations promote the idea of a primordial origin for magnetic fields, i.e. fields generated in the early Universe before structure formation. There are a number of theoretical mechanisms proposed to generate primordial magnetic fields; such mechanisms for example involve inflation [7], first-order phase transitions [8], or vorticity generation [9,10].

If primordial magnetic fields were indeed generated, they would suffer decay on small scales due to magnetohydrodynamics (MHD) effects [11–13]. The dissipation of magnetic fields injects energy into the plasma, and if this occurs in the early Universe when the cosmic microwave background (CMB) is being formed [14], distortions to its blackbody spectrum can be generated [15–24]. Distortions to the CMB blackbody spectrum come in different types depending on the epoch of energy injection. At relatively early times a μ-type distortion can be generated, where the photon Bose-Einstein distribution develops a nonvanishing chemical potential. Whereas at later times a Compton y-parameter can be generated giving a y-type distortion. Mixed distortions are also possible [25]. Any mechanism which injects energy into the plasma in the early Universe has the potential to generate such distortions. Other mechanisms in the early Universe include the dissipation of primordial acoustic waves [18,26], decaying or annihilating relic particles [27–29], and the evaporation of primordial black holes or cosmic strings [30,31].

In this paper we consider magnetic fields generated by some causal process in the early Universe. In particular we consider the possibility of magnetic fields generated by first-order phase transitions at either the electroweak (EW) or the QCD scale [8]. The spectrum on large scales for magnetic fields generated in such a process is highly constrained due to causality reasons [32]. The slope of the large scale spectrum also determines the subsequent MHD evolution of magnetic energy and coherence scale [12,13,33]. As the small scales dissipate into heat in a turbulent plasma, the peak of the spectrum moves down along the large scale spectrum [12,13,34,35]. The amplitude of magnetic helicity also determines the evolution of magnetic fields. Helicity conservation in the early Universe slows down the decay rate of fully helical fields compared to nonhelical fields and leads to an inverse cascade of energy from small scales to large scales [11,12]. Hence, causally generated magnetic fields and their initial helicity fraction can be constrained by CMB spectral distortions.

In Sec. II we use the results of Refs. [12,13,33] to determine the decay rates of magnetic fields as functions of their initial strength, coherence length, and initial helicity fraction. From these decay rates, in Sec. III, we calculate the CMB spectral distortions generated and analyze the parameter space. We conclude in the final section.

II. DECAY OF MAGNETIC FIELDS IN THE EARLY UNIVERSE

In order to calculate the CMB spectral distortions, we need to know the energy injected into the primordial

*jwagstaff@hs.uni-hamburg.de

plasma. For decaying magnetic fields, the energy injection rate is given by [20,21]

$$\frac{\mathrm{d}Q}{\mathrm{d}t} \equiv -a^{-4}\frac{\mathrm{d}\tilde{\rho}_B}{\mathrm{d}t}, \tag{1}$$

where $\tilde{\rho}_B$ is the comoving energy density, i.e. $\tilde{\rho}_B \equiv a^4\rho_B$. The averaged magnetic energy density is obtained by integrating over the *local* energy density $u_B = \tilde{\mathbf{B}}^2/8\pi$; here $\tilde{\mathbf{B}} \equiv a^2\mathbf{B}$ is the comoving magnetic field,

$$\tilde{\rho}_B = \frac{1}{V}\int u_B \mathrm{d}\mathbf{r} = \frac{1}{8\pi}\int |\tilde{\mathbf{B}}(\mathbf{k})|^2 \mathrm{d}\mathbf{k} \equiv \tilde{\rho}\int M_k \mathrm{d}k, \tag{2}$$

where $\tilde{\rho}$ is the total comoving energy density and M_k is the magnetic spectral energy. Here, we emphasize that the spectrum on large scales, parametrized by $M_k \propto k^{n+2}$, for causally generated magnetic fields is constrained by $n \geq 2$ [32]. The most shallow, and expected, scaling $n = 2$ is also confirmed by numerical simulations giving $M_k \propto k^4$ [34,36]. Assuming that the magnetic energy is concentrated at the *integral* scale (index I), which defines the peak of the spectrum in Fourier space, we can write $\tilde{\rho}_B = \tilde{\rho}\int kM_k \mathrm{d}\ln k \simeq \tilde{\rho}k_I M_I$, adopting the conventions of Ref. [34] where the wave vector k is also comoving. Since the photon energy density scales as $\rho_\gamma \propto a^{-4}$, we can write

$$\rho_\gamma^{-1}\frac{\mathrm{d}Q}{\mathrm{d}z} = -\rho_{\gamma,0}^{-1}\frac{\mathrm{d}\tilde{\rho}_B}{\mathrm{d}z} \simeq -\rho_{\gamma,0}^{-1}\frac{\mathrm{d}(\tilde{\rho}k_I M_I)}{\mathrm{d}z}, \tag{3}$$

where $a_0 \equiv a(T_0) = 1$ today.

The magnetic field strength B_I and coherence length L_I (identified as $2\pi/k_I$) evolve during the radiation dominated era due to turbulent MHD effects [12,37–39]. In the following, we quote the results from the detailed analytical and numerical analysis in Refs. [12,13,33]. The evolution of the field strength and coherence length depends on the state of the plasma and on the properties of the magnetic field, in particular its helicity. The average helicity density is given by

$$h_B = \frac{1}{V}\int (\mathbf{A}\cdot\mathbf{B})\mathrm{d}\mathbf{r} = \rho\int \mathcal{H}_k \mathrm{d}k, \tag{4}$$

where $\mathbf{B} = \nabla \times \mathbf{A}$. For a magnetic field with helicity, on any given scale k, there is a *realizability* condition given by $|\mathcal{H}_k| \leq 8\pi M_k/k$, where the helical spectrum $\mathcal{H}_k$ is defined following the conventions of Ref. [35]. From the above, we can define $f \equiv k\mathcal{H}_k/8\pi M_k$ as the helicity fraction, where $f = 0$ for the nonhelical case and $f = 1$ for the maximally helical case. The helicity density is a useful quantity since it is conserved in the early Universe $h_B \simeq \text{const}$ when the conductivity $\sigma = 1/4\pi\eta \to \infty$ [40], and the conservation of magnetic helicity determines the evolution of the magnetic field strength and coherence length.

In the turbulent regime, where kinetic Reynolds numbers are large $R_e \gg 1$, the general decay law for the magnetic energy is $M_I \propto a^{-2(n+2)/(n+5)}$ and for the comoving integral scale $L_I \propto a^{2/(n+5)}$ [12,34,35]; hence, $\tilde{B}_I \propto a^{-5/7}$, $k_I \propto a^{-2/7}$, and $\tilde{\rho}_B \propto a^{-10/7}$, where $n = 2$ is used due to causality constraints for the large scale spectrum [12,32,34,35]. These decay laws for nonhelical magnetic fields, where the helicity fraction $f \ll 1$ if not zero, are obtained through analytical considerations in Refs. [12,13,33] and confirmed numerically in Ref. [12]. If the magnetic field has nonzero helicity, the helicity density in this case would grow as $\mathcal{H}_I \propto a^{2/7}$, and eventually the magnetic field would become fully helical $f = 1$. The conservation of magnetic helicity ensures the relation $\tilde{\rho}_B \propto \tilde{B}_I^2 \propto k_I$. The decay of magnetic fields slows down in the fully helical case, and the decay rate becomes independent of the shape of the large scale spectrum n. For the maximally helical case, we find $\tilde{B}_I \propto a^{-1/3}$, $k_I \propto a^{-2/3}$, and $\tilde{\rho}_B \propto a^{-2/3}$. We can summarize the above turbulent damping (TD) decay laws by

$$(\mathrm{TD}):\ \tilde{\rho}_B \propto a^{-2\frac{p+5}{p+7}}, \qquad L_I \propto a^{\frac{2}{p+7}}, \tag{5}$$

where $p = 0$ for nonhelical fields and $p = -4$ for maximally helical fields.

Here, we note that an apparent inverse transfer of magnetic energy has been numerically observed for the nonhelical case. This effect leads to a weaker evolution for nonhelical magnetic fields in the turbulent regime $\tilde{B}_I \propto a^{-1/2}$, $k_I \propto a^{-1/2}$, and $\tilde{\rho}_B \propto a^{-1}$, i.e. $p = -3$ above, giving $B_I \propto L_I^{-1}$ [41] (see also Ref. [42]). This is potentially a very interesting and exciting new development in turbulent MHD. However, this is a numerically observed effect under the conditions of high resolutions and magnetically dominant turbulence [36]. The condition of magnetically dominant turbulence is perhaps not satisfied in the early Universe. Magnetogenesis at first-order phase transitions typically produce a lot of turbulent kinetic energy. The generated magnetic field, through dynamo action, comes into equipartition with the kinetic energy but is unlikely to dominate over the kinetic energy; see for example Ref. [8]. Furthermore, in the study by Ref. [36], it seems that the inverse transfer is less efficient for large Prandtl numbers, but the Prandtl numbers in the early Universe are huge. In any case, we will also investigate the CMB spectral distortions considering these scalings to complete the study.

In the viscous regime, where $R_e < 1$, during particle diffusion, the rapidly growing particle mean free path means that the dissipative time scale is increasing faster than the Hubble time H^{-1}. This prevents further dissipation of magnetic energy, and so the magnetic energy freezes out and remains constant [12],

$$(\mathrm{VF}):\ \tilde{\rho}_B \simeq \mathrm{const}, \qquad L_I \simeq \mathrm{const}. \tag{6}$$

The above evolution in the viscous freezing (VF) stage occurs regardless of magnetic helicity. However, as the mean free path increases further, particles begin to free stream out of overdensities. In this case, the interaction between the fluid and the background is described by a drag force, which is a decreasing function of time. This leads to a situation where the magnetic dissipative time scale can become smaller than the Hubble time once again, and magnetic energy decay can start again [12,13]. The drag force due to the free streaming of neutrinos becomes ineffective at approximately the freeze-out of neutrinos, i.e. when their mean free path becomes larger than the Hubble scale. The dissipation due to photon drag is efficient until photon freeze-out at $T \simeq 0.26$ eV when recombination commences. The decay of magnetic fields due to viscous photon free streaming is given by $k_I \propto a^{-3/(n+5)}$ and $\tilde{\rho}_B \propto a^{-3(n+3)/(n+5)}$ [12]. With $n = 2$, we find $\tilde{B}_I \propto a^{-15/14}$, $k_I \propto a^{-3/7}$, and $\tilde{\rho}_B \propto a^{-15/7}$, which is a faster decay than in the turbulent case and faster than in the case of a maximally helical field. For maximally helical fields, the relation $\tilde{\rho}_B \propto k_I$ again holds, and the decay due to free-streaming photons is $\tilde{B}_I \propto a^{-1/2}$, $k_I \propto a^{-1}$, and $\tilde{\rho}_B \propto a^{-1}$. We can summarize the above viscous damping (VD) decay laws by

$$(\mathrm{VD}):\ \tilde{\rho}_B \propto a^{-3\frac{p+5}{p+7}}, \qquad L_I \propto a^{\frac{3}{p+7}}, \tag{7}$$

where $p = 0$ for nonhelical fields and $p = -4$ for maximally helical fields.

In order to calculate the CMB spectral distortions due to decaying magnetic fields, we have to know to which of the above phases of evolution the μ and y eras correspond. For this, we must understand when these phases begin and end, which is what we do in the next section.

A. End of the turbulent damping stage

When the magnetic fields are first generated, for example by a first-order phase transition, the magnetic energy is expected to come into equipartition with the kinetic energy (see Ref. [39] for a detailed analysis of this mechanism). At the time of the EW or QCD scale, it can be shown that the kinetic Reynolds numbers are very large in this case and the plasma is highly turbulent. Hence, magnetogenesis ends with the plasma in a turbulent state. We now calculate T_{EoT}, the temperature corresponding to the end of turbulence. Turbulence ends when the kinetic Reynolds number decreases to $R_e \sim 1$, and hence the end-of-turbulence temperature is obtained through

$$R_e(T_{\mathrm{EoT}}) \sim 1. \tag{8}$$

At the time of the EW or QCD scale, the plasma viscosity is generated by neutrinos, since at this time they are the particles which are the most efficient at transporting momentum and heat [12]. But as the Universe expands and cools, the neutrino mean free path increases which increases the plasma viscosity. Therefore, due to neutrinos, the plasma goes from a turbulent state to a viscous state up until the neutrinos decouple at $T_{\nu\mathrm{dec}} \simeq 2.6$ MeV. The evolution of magnetic energy and its coherence length in the turbulent stage due to neutrinos followed by the viscous stage before neutrino decoupling can be well approximated by only considering a turbulent damping stage throughout that epoch [12]. In our calculations, we use this simplifying approximation.

After neutrino decoupling, we are in the photon era, when photons generate the plasma shear viscosity η_s. In this case, the Reynolds number is given by [12]

$$R_e(l) = \frac{v_l^{\mathrm{rms}} l}{\eta_s} = \frac{5 g_*(T)}{g_\gamma} \frac{v_l^{\mathrm{rms}} l_c}{l^\gamma_{\mathrm{mfp},c}(T)}, \tag{9}$$

for velocity fluctuations v_l^{rms} correlated on some physical scale l. Here, g_* and g_γ are the total and component numbers of effective relativistic degrees of freedom. We apply the above from the time of neutrino decoupling at $T_{\nu\mathrm{dec}} \simeq 2.6$ MeV to the time of matter-radiation equality at $T_{\mathrm{eq}} \simeq 1$ eV. In this epoch, the comoving photon mean free path is given by [43]

$$l^\gamma_{\mathrm{mfp},c} \simeq \frac{a^{-1}}{\sigma_T \sqrt{n_{\mathrm{pair}}^2 + n_e^2}}, \tag{10}$$

where $\sigma_T = 8\pi\alpha^2/3m_e^2$ is the Thomson cross section, $\alpha \approx 1/137$ is the fine structure constant, and m_e is the electron mass. The number densities n_{pair} and n_e of $e^\pm$ pairs and free electrons respectively are given by [43]

$$n_{\mathrm{pair}} \approx \left(\frac{2 m_e T}{\pi}\right)^{\frac{3}{2}} \exp\left(-\frac{m_e}{T}\right)\left(1 + \frac{15}{8}\frac{T}{m_e}\right), \tag{11}$$

$$n_e = X_e \frac{\Omega_b \rho_0}{m_{\mathrm{pr}}} \left(\frac{T}{T_0}\right)^3, \tag{12}$$

where m_{pr} is the proton mass, the baryon fraction and present day density product is $\Omega_b \rho_0 \simeq 1.81 \times 10^{-12}\ \mathrm{eV}^4$ [44], $T_0 \simeq 2.725$ K is the present day photon temperature, and the ionization fraction is $X_e = 1$ in the radiation dominated era. Following the usual assumption that in the turbulent regime $R_e(L_I) \gg 1$ there is equipartition between magnetic and kinetic energy on all scales up to the integral scale, i.e.

$$(v_k^{\mathrm{rms}})^2 = \Gamma \frac{(\tilde{B}_k^{\mathrm{rms}})^2}{4\pi\tilde{\rho}} \quad \text{for } k \geq k_I. \tag{13}$$

Numerical simulations show that there is almost exact equipartition, i.e. $\Gamma \approx 1$ for nonhelical fields, which is slightly reduced to $\Gamma \approx 10^{-1}$ for maximally helical fields [12]. Therefore, we find on the integral scale

$$R_e(L_I, T) \simeq \sqrt{\Gamma}\frac{5g_*}{g_\gamma}\frac{L_I}{l^\gamma_{\mathrm{mfp},c}}\left(\frac{2\tilde{\rho}_B}{\tilde{\rho}}\right)^{\frac{1}{2}}, \tag{14}$$

which is to be evaluated from the time of neutrino decoupling. To connect the magnetic energy density with the coherence length, we use the approximation discussed below Eq. (8). Hence, we can use Eq. (5) to find $L_I\sqrt{\tilde{\rho}_B} = L_{I,*}\sqrt{\tilde{\rho}_{B,*}}(T/T_*)^{(p+3)/(p+7)}$, where the index $*$ denotes the epoch of magnetogenesis. With the above, the Reynolds number is

$$R_e(L_I, T) \simeq \sqrt{2\Gamma\varepsilon}\beta\frac{5g_*}{g_{\nu,\gamma}}\frac{\lambda^{\max}_{B,*}}{l^\gamma_{\mathrm{mfp},c}}\left(\frac{T}{T_*}\right)^{\frac{p+3}{p+7}}, \tag{15}$$

where we have defined $\varepsilon \equiv \tilde{\rho}_{B,*}/\rho_{\gamma,0} \simeq \tilde{\rho}_{B,*}/\tilde{\rho}$. Here, the maximal magnetic energy $\varepsilon = 1$ corresponds to $u_B = \tilde{\rho}/2$, i.e. a maximum magnetic field strength of

$$\tilde{B}^{\max}_{\lambda,*} \equiv \sqrt{4\pi\tilde{\rho}} \simeq 3\times 10^{-6}\ \mathrm{G}, \tag{16}$$

where the radiation here is taken to be the CMB photons [12]. In the above, we have also defined $\beta \equiv \lambda_{B,*}/\lambda^{\max}_{B,*}$, and we have identified the integral scale $L_{I,*}$ with the magnetic field coherence length $\lambda_{B,*}$. For magnetic fields generated at a time during the radiation dominated era (in contrast to inflationary magnetogenesis), the basic constraint on the coherence length is the horizon size at the time of magnetogenesis

$$\lambda_{B,*} \le \lambda^{\max}_{B,*} \equiv \frac{1}{aH}\bigg|_*. \tag{17}$$

The horizon size is 2×10^{-10} Mpc and 3×10^{-7} Mpc at the electroweak and QCD phase transitions respectively. To estimate the integral scale at the time of magnetogenesis $L_{I,*}$, we can assume that turbulence is effective such that the Alfvén eddy-turnover time $t_{A,*}$ is equal to the Hubble time [12], i.e.

$$t_{A,*} \equiv \frac{L}{v^{\mathrm{rms}}_{A,L}}\bigg|_* = \frac{1}{aH}\bigg|_*, \tag{18}$$

where $v^{\mathrm{rms}}_{A,L} \equiv \tilde{B}^{\mathrm{rms}}_L/\sqrt{4\pi\tilde{\rho}}$. With the above, we find that $\lambda_{B,*} = L_{I,*} = \sqrt{\varepsilon}/aH|_*$, and hence we can set $\beta = \sqrt{\varepsilon}$ in Eq. (15) above.

The end-of-turbulence temperature, obtained through $R_e(T_{\mathrm{EoT}}) \sim 1$, can only be determined numerically; we cannot analytically invert the function in Eq. (15) due to the exponential in the photon mean free path. We find that $T_{\mathrm{EoT}} \simeq 2\times 10^4$ eV and 2×10^3 eV for nonhelical magnetic fields generated at the EW and QCD phase transitions, $T_* \simeq 100$ GeV and 200 MeV respectively, with $\beta = 1$ and $\varepsilon = 1$. Hence, the μ-era is within the viscous regime, since the μ-era commences at around $T_{\mu,i} \simeq 470$ eV. However, for maximally helical fields, it is possible that the plasma is still in a turbulent stage within the μ-era. The point here is that the magnetic field decay could be in the turbulent, viscous freezing or viscous damping regime depending on the initial conditions. This can be seen in the evolution plots in Fig. 1.

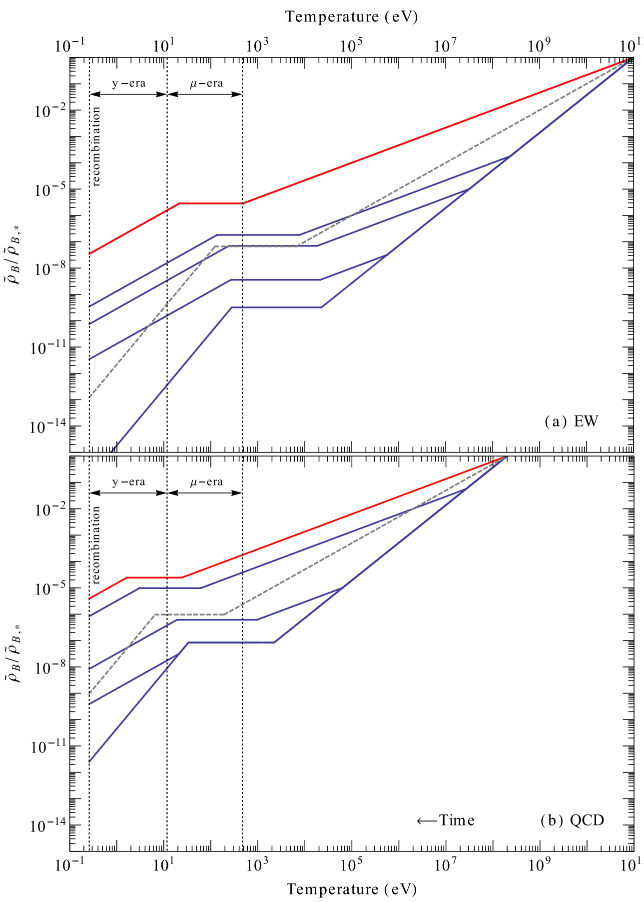

FIG. 1 (color online). In plots (a) and (b), we show the evolution of magnetic energy from the time of magnetogenesis (at the EW and QCD scales respectively) to recombination. In plots (a) and (b), the (solid, blue) lines from top to bottom correspond to initial helicity fractions $f_* = \{10^{-3}, 10^{-4}, 10^{-6}, < 10^{-14}\}$ and $f_* = \{10^{-1}, 10^{-4}, 10^{-6}, < 10^{-14}\}$ respectively. The maximally helical case $f_* = 1$ (solid, red) is also shown. We also show (dashed, gray lines) the evolution of nonhelical magnetic fields with an inverse transfer of energy [see the discussion below Eq. (5)]. In all the above cases we consider $\varepsilon \equiv \tilde{\rho}_{B,*}/\rho_{\gamma,0} \approx 1$, which corresponds to an initial field strength of $\tilde{B}_{\lambda,*} \simeq 3\times 10^{-6}$ G, with $\varepsilon < 1$ the evolution history also changes.

B. Start of the viscous damping stage

The magnetic energy and coherence length stop evolving in the viscous regime when particles are diffusing $l_{\mathrm{mfp},c} \ll L$ [see above Eq. (6)]. The viscous damping stage occurs when photons begin to free stream $l_{\mathrm{mfp},c} \gg L$. The start of the viscous damping stage (index "vd") is determined by the condition [12]

$$\tau_{\mathrm{visc.free}}(T_{\mathrm{vd}}) = H^{-1}(T_{\mathrm{vd}}), \tag{19}$$

where the viscous free-streaming time scale is given by $\tau_{\mathrm{visc.free}} = \alpha_\gamma L^2/v_A^2$. Here, the drag term on the fluid due to the occasional scattering of photons with the fluid particles is given by [12]

$$\alpha_\gamma \simeq \frac{4}{3}\frac{1}{l_{\mathrm{mfp}}}\frac{\rho_\gamma}{\rho_b}, \tag{20}$$

where ρ_b is the baryon density. The Alfvén velocity is given by $v_A^2 \simeq 2\rho_B/\rho_b$, since at this time the photons are decoupled from the fluid. Magnetic dissipation due to photon drag is shown to be efficient until photon decoupling [12].

Hence, we can solve Eq. (19) for T_{vd}, the temperature at the start of the viscous damping due to free-streaming photons. We find

$$T_{\mathrm{vd}}^3 \simeq \frac{9}{16\pi^2\alpha^2}\sqrt{\frac{90}{g_{*,\mathrm{vd}}}}\frac{m_P m_{\mathrm{pr}} m_e^2 T_0}{X_{e,\mathrm{vd}}\Omega_b\rho_0}\left(\frac{T_{\mathrm{EoT}}}{\lambda_{B,*}^{\mathrm{max}} T_*}\right)^2, \tag{21}$$

which is valid for $T \lesssim 10^4$ eV when the photon mean free path can be well approximated by $l_{\mathrm{mfp}}^\gamma \simeq 1/\sigma_T n_e$.

The evolution of magnetic energy due to MHD turbulence occurs approximately until the time of recombination (index "rec"), when the field configuration falls on the line given by [12,37]

$$B_{\lambda,\mathrm{rec}} \simeq 8\times 10^{-8}\frac{\lambda_{B,\mathrm{rec}}}{\mathrm{Mpc}}\,\mathrm{G}. \tag{22}$$

This line corresponds to the largest eddies being processed at recombination $1/(aH)|_{\mathrm{rec}} \simeq \lambda/v_A$ with v_A the Alfvén speed [12,45]. Beyond this epoch, the evolution of the field strength and coherence length essentially ceases, with only a logarithmic scaling [12], and the magnetic fields become frozen into the plasma. Hence, magnetic fields generated during the radiation era evolve until recombination where their final field strength and coherence length configuration is given by Eq. (22). This field strength and coherence length configuration at recombination also gives the values observed today $B_{\lambda,\mathrm{rec}} \approx B_0$ and $\lambda_{B,\mathrm{rec}} \approx \lambda_B$, since the field strength and coherence length do not evolve significantly in the matter dominated Universe.

We now have all the necessary ingredients to characterize the full evolution of magnetic fields in the radiation dominated epoch. Exemplary evolution histories of magnetic energy for varying initial conditions can be seen in the plots of Fig. 1, where different initial conditions $\tilde{B}_{\lambda,*}$, $\lambda_{B,*}$, and f_* lead to different histories and hence different decay rates during the μ- and y-eras.

III. SPECTRAL DISTORTIONS FROM DECAYING MAGNETIC FIELDS

At high temperatures, corresponding to $z \gtrsim 2\times 10^6$, the blackbody spectrum of the CMB [14] is formed from bremsstrahlung and double-Compton scattering (see for example Ref. [20] and references therein). As the redshift drops below 2×10^6, these interactions become inefficient at restoring the blackbody spectrum if additional energy is injected into the plasma and distortions could be imprinted from then on. In the early stage $2\times 10^6 \gtrsim z \gtrsim 5\times 10^4$, the elastic-Compton scattering is efficient enough, and the spectral distortion comes in the form of a nonvanishing chemical potential μ. This μ-type CMB spectral distortion is generated if thermal energy is injected into the plasma during the μ-era defined above. The rate of change of the chemical potential μ is determined by [16–19]

$$\frac{\mathrm{d}\mu}{\mathrm{d}t} = -\frac{\mu}{t_{\mathrm{DC}}(z)} + \frac{1.4}{3}\rho_\gamma^{-1}\frac{\mathrm{d}Q}{\mathrm{d}t}, \tag{23}$$

where $\mathrm{d}Q/\mathrm{d}t$ is the energy injection rate. Here, the time scale for double-Compton scattering is

$$\frac{t_{\mathrm{DC}}(z)}{\mathrm{s}} = \frac{2.06\times 10^{33}}{\Omega_b h^2}\left(1-\frac{1}{2}Y_P\right)^{-1} z^{-\frac{9}{2}}, \tag{24}$$

and $Y_P = 0.24$ is the primordial helium mass abundance [46]. The solution to Eq. (23) is given by [20]

$$\mu = \frac{1.4}{3}\int_{z_i}^{z_{\mathrm{end}}}\frac{\mathrm{d}z}{\rho_\gamma}\frac{\mathrm{d}Q}{\mathrm{d}z}\exp\left[-\left(\frac{z}{z_{\mathrm{DC}}}\right)^{\frac{5}{2}}\right], \tag{25}$$

where

$$z_{\mathrm{DC}} \equiv \frac{1.97\times 10^6}{(1-\frac{1}{2}\frac{Y_P}{0.24})^{\frac{2}{5}}}\left(\frac{\Omega_b h^2}{0.0224}\right)^{-\frac{2}{5}} \tag{26}$$

and where $z_i = 2\times 10^6$ and $z_{\mathrm{end}} = 5\times 10^4$ define the start and end of the μ-era.

A. CMB μ-type distortions from decaying magnetic fields

From the full evolution history of magnetic fields shown in Fig. 1, we can see that, in most cases, the plasma is in the viscous regime during the μ-era. This is true in most cases except for fields generated at the QCD scale if the initial helicity fraction is large enough. For analytical purposes, let us first consider the viscous damping law, from which we can write

$$\tilde{\rho}_B(z) = \tilde{\rho}_{B,\mathrm{vd}} \left(\frac{1+z}{1+z_{\mathrm{vd}}} \right)^{3\frac{p+5}{p+7}}, \tag{27}$$

where $\tilde{\rho}_{B,\mathrm{vd}}$ indicates the magnetic energy at the start of the viscous damping stage. Here, we also use $a \propto 1/T$ for the photon temperature and $T = T_0(1+z)$. Since the magnetic energy is frozen out from the time of the end of turbulence (EoT) to the start of the viscous damping stage, we can set $\tilde{\rho}_{B,\mathrm{vd}} \simeq \tilde{\rho}_{B,\mathrm{EoT}}$, and hence we find

$$\begin{aligned} \rho_\gamma^{-1} \frac{\mathrm{d}Q}{\mathrm{d}z} &= -\rho_{\gamma,0}^{-1} \frac{\mathrm{d}\tilde{\rho}_B}{\mathrm{d}z} \\ &\simeq -3 \frac{p+5}{p+7} \frac{\tilde{\rho}_{B,\mathrm{EoT}}}{\rho_{\gamma,0}} (1+z_{\mathrm{vd}})^{-3\frac{p+5}{p+7}} (1+z)^{2\frac{p+4}{p+7}}. \end{aligned} \tag{28}$$

To calculate $\tilde{\rho}_{B,\mathrm{EoT}}$, we consider the era when turbulence is generated by photons after neutrino decoupling. As already argued in Sec. II A, we can trace the evolution of the magnetic energy all the way back to the time of magnetogenesis using the turbulent decay law given in Eq. (5). This is possible since the turbulent stage due to neutrinos followed by the viscous stage before neutrino decoupling can be well approximated by only considering a turbulent damping stage throughout the epoch [12]. Hence, using the turbulent damping decay law, we can write

$$\tilde{\rho}_{B,\mathrm{EoT}} = \tilde{\rho}_{B,*} \left(\frac{T_{\mathrm{EoT}}}{T_*} \right)^{2\frac{p+5}{p+7}}. \tag{29}$$

In the cases where the viscous regime starts before the μ-era, i.e. $T_{\mathrm{EoT}} \geq T_{\mu,i}$, we can use Eqs. (28) and (29) to estimate the μ-type distortion from Eq. (25), and we find

$$\begin{aligned} \mu = &-\frac{7}{5} \frac{p+5}{p+7} \left(\frac{\tilde{\rho}_{B,*}}{\rho_{\gamma,0}} \right) \left(\frac{T_{\mathrm{EoT}}}{T_*} \right)^{2\frac{p+5}{p+7}} (1+z_{\mathrm{vd}})^{-3\frac{p+5}{p+7}} \\ &\times \int_{z_i}^{z_{\mathrm{end}}} \mathrm{d}z (1+z)^{2\frac{p+4}{p+7}} \exp\left[-\left(\frac{z}{z_{\mathrm{DC}}} \right)^{\frac{5}{2}} \right], \end{aligned} \tag{30}$$

where we integrate from $z_i = z_{\mathrm{vd}}$ to z_{end}. In the cases where the turbulent regime has not ended by the start of the μ-era, e.g. applicable for fully helical magnetic fields generated at the QCD scale with $\varepsilon \simeq 1$–10^{-2} as can be seen in Fig. 1, we find

$$\begin{aligned} \mu = &-\frac{14}{15} \frac{p+5}{p+7} \left(\frac{\tilde{\rho}_{B,*}}{\rho_{\gamma,0}} \right) \left(\frac{T_0}{T_*} \right)^{2\frac{p+5}{p+7}} \\ &\times \int_{z_i}^{z_{\mathrm{end}}} \mathrm{d}z (1+z)^{\frac{p+3}{p+7}} \exp\left[-\left(\frac{z}{z_{\mathrm{DC}}} \right)^{\frac{5}{2}} \right], \end{aligned} \tag{31}$$

where we integrate from z_i to $z_{\mathrm{end}} = z_{\mathrm{EoT}}$.

Equations (30) and (31) above are valid for either nonhelical fields ($p = 0$) or maximally helical fields ($p = -4$). Since we are interested in different initial conditions, in particular varying initial helicity fractions f_*, we must consider the full evolution history to calculate the spectral distortions. This is done numerically, and the results are shown in Figs. 2 and 3 for magnetic fields generated at the EW and QCD scales respectively. The μ-type spectral distortion varies with $\mu = \mu(\varepsilon, T_*, f_*)$. In order to maximize this distortion, we can set the maximal value $\varepsilon \equiv \tilde{\rho}_{B,*}/\rho_{\gamma,0} \approx 1$ at the time of magnetogenesis, which corresponds to an initial field strength of $\tilde{B}_{\lambda,*} \simeq 3 \times 10^{-6}$ G. From Eq. (30), we see that if $\varepsilon < 1$ then T_{EoT} will be larger, thereby increasing the chemical potential. However, T_{EoT} does not depend so strongly on ε, and therefore ε should be maximized in order to maximize

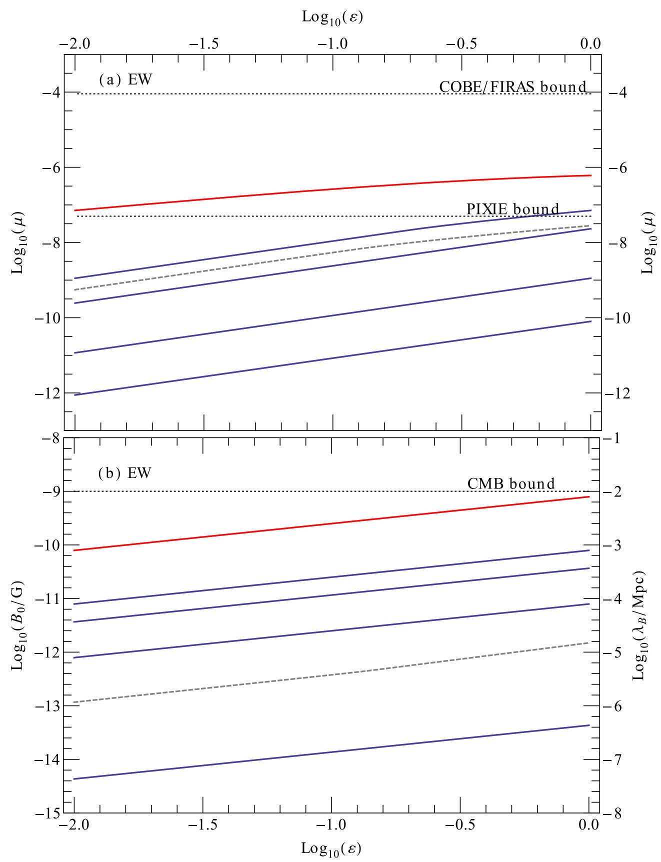

FIG. 2 (color online). EW scale: In plot (a), we show the μ-type distortion generated due to the decay of magnetic energy initially generated at the EW scale. Here, we plot the spectral distortion μ vs ε, where $\varepsilon \equiv \tilde{\rho}_{B,*}/\rho_{\gamma,0} \approx 1$ corresponds to an initial field strength $\tilde{B}_{\lambda,*} \simeq 3 \times 10^{-6}$ G. The (solid, blue) lines from top to bottom, in both plots, correspond to initial helicity fractions $f_* = \{10^{-3}, 10^{-4}, 10^{-6}, < 10^{-14}\}$. The maximally helical case $f_* = 1$ (solid, red) is also shown. In plot (b), we show the final field strength B_0 and coherence length λ_B that would be observed today, i.e. after MHD turbulent decay; see Eq. (22). We also show the approximate constraint on magnetic fields from CMB observations, $B_0 \lesssim 10^{-9}$ G; see Ref. [48] and references therein. The results for nonhelical magnetic fields with an inverse transfer of energy [see the discussion below Eq. (5)] are also shown (dashed, gray lines).

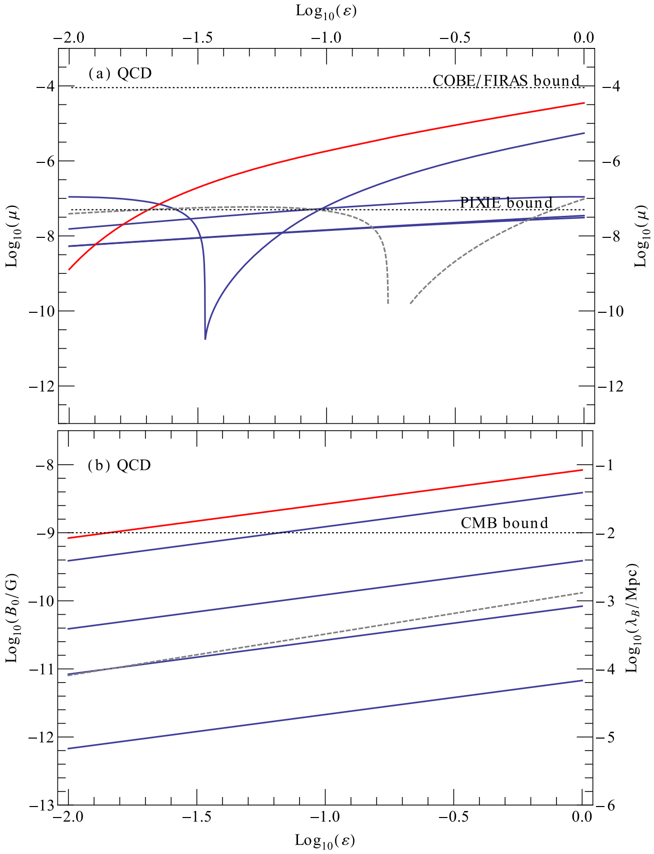

FIG. 3 (color online). QCD scale: In plot (a), we show the μ-type distortion generated due to the decay of magnetic energy initially generated at the QCD scale. Here, we plot the spectral distortion μ vs ε, where $\varepsilon \equiv \tilde{\rho}_{B,*}/\rho_{\gamma,0} \approx 1$ corresponds to an initial field strength $\tilde{B}_{\lambda,*} \simeq 3 \times 10^{-6}$ G. The (solid, blue) lines from top to bottom, in both plots, correspond to initial helicity fractions $f_* = \{10^{-1}, 10^{-4}, 10^{-6}, < 10^{-14}\}$. The maximally helical case $f_* = 1$ (solid, red) is also shown. In plot (b), we show the final field strength B_0 and coherence length λ_B that would be observed today, i.e. after MHD turbulent decay; see Eq. (22). We also show the approximate constraint on magnetic fields from CMB observations, $B_0 \lesssim 10^{-9}$ G; see Ref. [48] and references therein. The results for nonhelical magnetic fields with an inverse transfer of energy [see the discussion below Eq. (5)] are also shown (dashed, gray lines). Here, we comment on the seemingly strange behavior of the plot for $f_* = 10^{-1}$ in the QCD case (also applicable to the nonhelical inverse transfer case, gray dashed line). As ε decreases, the onset of the viscous freezing regime begins earlier. For a certain value of ε, the start of the viscous freezing regime coincides with the start of the μ-era, and hence there is practically no magnetic energy decay in this time, and hence μ becomes very small. As ε decrease further, the start of the viscous damping stage occurs within the μ-era, and a large μ can once again be generated.

μ. Hence, with $\varepsilon = 1$, integrating Eq. (30), we obtain upper limits from Figs. 2 and 3. For fields generated at the EW phase transition $T_* \simeq 100$ GeV, see Fig. 2, with $f_* \lesssim 10^{-14}$, we find

$$|\mu| \lesssim 1 \times 10^{-10}. \tag{32}$$

The above satisfies the current COBE/FIRAS limit $|\mu| < 9 \times 10^{-5}$ [14] but will also not be detectable by a new PIXIE-like experiment which would place a new upper limit of $|\mu| < 5 \times 10^{-8}$ [47]. From this, we conclude that causally generated nonhelical magnetic fields at the electroweak phase transition will not produce any detectable CMB μ-type spectral distortions. This is true even if we consider the nonhelical inverse transfer effect seen in Refs. [36,41] and discussed below Eq. (5); see the gray dashed line in Fig. 2. For nonhelical fields generated at the QCD phase transition $T_* \simeq 200$ MeV, see Fig. 3, we obtain the upper limit $|\mu| \lesssim 3 \times 10^{-8}$, which satisfies the current COBE/FIRAS limit [14] and is very much on the limit of detectability by a new PIXIE-like experiment [47]. The results do not change much if we consider the nonhelical inverse transfer effect discussed below Eq. (5); see the gray dashed line in Fig. 3.

The situation is quite different if magnetic helicity is introduced. As can be seen from Figs. 2 and 3, if the initial helicity fraction $f_* \gtrsim (10^{-3}\text{–}10^{-4})$, then PIXIE-observable μ-type distortions can be generated. We also note that for maximally helical fields $f_* = 1$ the current COBE/FIRAS limit is not broken [14], so that we cannot constrain primordial helicity from current data. If a future PIXIE-like experiment positively detects a μ-type spectral distortion, then primordial magnetic helicity can be constrained.

Here, we note that in Refs. [20,21] authors considered the evolution of the photon diffusion scale, i.e. the Silk damping scale, as the evolution of the damping scale k_d. Where we can write $k_I \approx k_d$ with an equivalent evolution. However, in these works, the authors only considered a scale-invariant Alfvén velocity, corresponding to scale-invariant spectrum $n = -3$, and this gives the much faster evolution of the integral scale $k_I \propto a^{-3/2}$ (for nonhelical fields with $p = 0$) as seen in their paper [20]. However, the magnetic energy is still considered to evolve along the large scale spectrum, i.e. $\tilde{B}_I \propto k_I^{5/2}$, and hence the authors find a much faster magnetic field decay rate $\tilde{\rho}_B \propto a^{-15/2}$. With this decay rate, the chemical potential scales as $\mu \propto \int dz(1+z)^{13/2} e^{-(z/z_{\mathrm{DC}})^{5/2}}$ as seen in their paper [20]. This fast magnetic field decay rate leads to a huge overestimation of the generated chemical potential for the causally generated magnetic fields. In our study, as can be seen in Figs. 2 and 3, the maximum possible magnetic energy $\varepsilon = 1$, which corresponds to $\tilde{B}_{\lambda,*} \simeq 3 \times 10^{-6}$ G at magnetogenesis, does not overgenerate spectral distortions. However, in the work of Ref. [20], an upper limit of $\sim 10^{-11}$ nG on the field strength of nonhelical magnetic fields is obtained due to current spectral distortions constraints.

B. CMB y-type distortions from decaying magnetic fields

After the end of the μ-era, for $z \lesssim 5\times 10^4$, the elastic Compton scattering becomes ineffective. From then on, the spectral distortion becomes a y type, i.e. defined by the Compton y-parameter [18]. It is possible that intermediate distortions between μ and y type are generated, where the exact shape of the spectral distortions can be used to identify heating mechanisms [25,28]. However, for the purpose of this paper, it is sufficient to only calculate the μ and y distortions in order to estimate the effects of magnetic helicity.

First, we consider the contribution to the y-distortion before decoupling, when the baryonic fluid is still tightly coupled to the photons. The Compton parameter in this case is calculated by

$$y = \frac{1}{12}\int_{z_{\rm end}}^{z_{\rm dec}} \frac{dz}{\rho_\gamma}\frac{dQ}{dz}, \tag{33}$$

where $z_{\rm end} \simeq 5\times 10^4$ is the end of the μ-era and hence the start of the y-era and $z_{\rm dec} \simeq 1088$ for the time of decoupling. We can see from the plots in Fig. 1 that in all cases, for magnetic fields generated at the EW or QCD scale and for any initial helicity fraction, the plasma is in a viscous state (viscous freezing or viscous damping) in the y-era before decoupling. Hence, as a first approximation for the maximum y-type distortion generated in this time, we can assume the viscous damping law given in Eq. (7) and a radiation dominated universe throughout this era. From Eq. (33) and the above considerations, we find

$$y = -\frac{1}{4}\frac{p+5}{p+7}\left(\frac{\tilde{\rho}_{B,*}}{\rho_{\gamma,0}}\right)\left(\frac{T_{\rm EoT}}{T_*}\right)^{2\frac{p+5}{p+7}} \times (1+z_{\rm vd})^{-3\frac{p+5}{p+7}}\int_{z_{\rm end}}^{z_{\rm dec}} dz(1+z)^{2\frac{p+4}{p+7}}. \tag{34}$$

Again, the above expression is valid for nonhelical fields ($p=0$) or maximally helical fields ($p=-4$). For varying initial helicity fractions f_*, a full calculation is done taking into account the full evolution history. The results are shown in the plots of Fig. 4.

For nonhelical fields, we can see from Fig. 4 that the maximum possible y-type distortion generated before decoupling, corresponding to fields generated at the QCD scale, is $y \lesssim 8\times 10^{-10}$. This result satisfies the current COBE/FIRAS limit $y \lesssim 1.5\times 10^{-5}$ [14] and is probably not detectable by a new PIXIE-like experiment, which would place a new lower bound at $y \lesssim 10^{-8}$ if not detected [47]. For nonhelical fields generated at the EW phase transition, there is little hope for detection with the maximum distortion at $y \simeq 3\times 10^{-14}$. We note that, if we consider the nonhelical inverse transfer effect discussed below Eq. (5) [see the gray dashed line in Fig. 4], the y-type distortion is still undetectable for fields generated at the EW scale; however, it seems now possible to detect a y-type distortion if the fields are generated at the QCD scale.

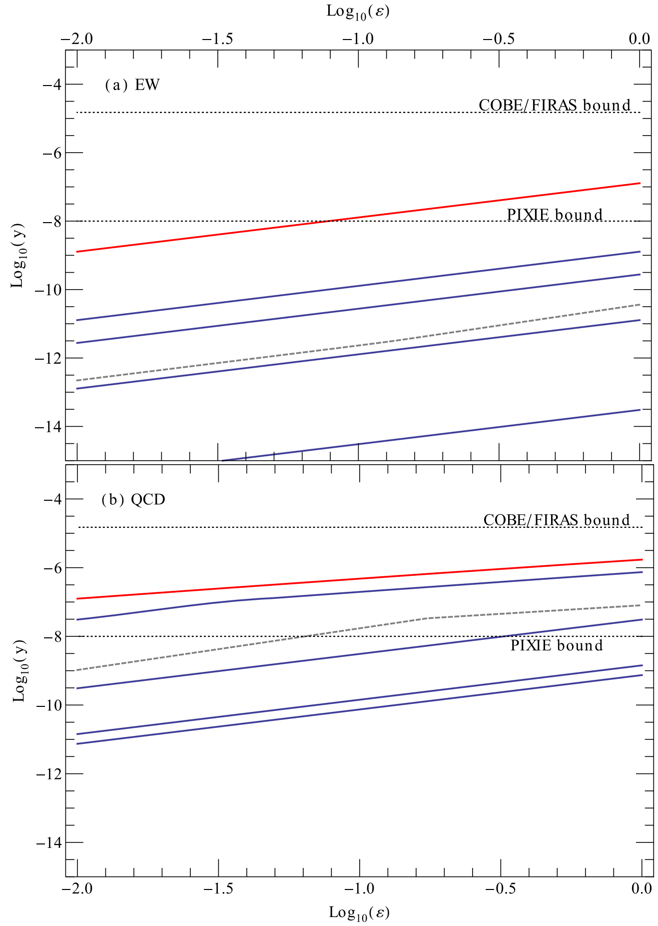

FIG. 4 (color online). In plots (a) and (b), we show the y-type distortion produced before decoupling due to the decay of magnetic energy initially generated at the EW and QCD scales respectively. Here, we plot the spectral distortion y vs ε, where $\varepsilon \equiv \tilde{\rho}_{B,*}/\rho_{\gamma,0} \approx 1$ corresponds to an initial field strength of $\tilde{B}_{\lambda,*} \simeq 3\times 10^{-6}$ G. In plots (a) and (b), the (solid, blue) lines from top to bottom correspond to initial helicity fractions $f_* = \{10^{-3}, 10^{-4}, 10^{-6}, < 10^{-14}\}$ and $f_* = \{10^{-1}, 10^{-4}, 10^{-6}, < 10^{-14}\}$ respectively. The maximally helical case $f_* = 1$ (solid, red) is also shown. The final field strength B_0 and coherence length λ_B that would be observed today, i.e. after MHD turbulent decay, see Eq. (22), are the same as in plots (b) of Figs. 2 and 3. We also show (dashed, gray lines) the results from nonhelical magnetic fields with an inverse transfer of energy [see the discussion below Eq. (5)].

For decaying helical magnetic fields, there is a possibility to generate a detectable y-type distortion before decoupling; see Fig. 4. However, since the y-era is later in the evolution history, magnetic fields have already substantially decayed and thus generate a smaller signal than that for the μ-type distortion. As discussed below, contributions to the y-type distortion can be generated after the decoupling of photons but will only provide similar constraints as the predecoupling contribution.

After decoupling, the CMB photons travel essentially freely until the present time. However, if the gas density and/or temperature is high enough, it is possible to generate spectral distortions after decoupling [24,28,49]. At low redshifts, heated-up gas in clumps and filaments at $T \sim 10^7$ K can produce a distortion $y \sim 10^{-6}$ over $l \sim H_0^{-1}$ via the Sunyaev-Zel'dovich effect [50]. There is also a contribution of $y \sim 10^{-7}$ from the reionization of the Universe [20]. At higher redshifts, with the presence of magnetic fields of order $B_0 \sim$ nG, the gas can be heated up to $T \sim 10^4$ K via turbulent magnetic decay and ambipolar diffusion [51–53]. The turbulent decay of magnetic fields in the postdecoupling era, when the Universe is matter dominated, occurs with a logarithmic scaling as opposed to the power-law scaling in the predecoupling era [51]. This means that the turbulent decay is a lot less sensitive to the primordial spectrum and helicity of the magnetic fields [20]. For this reason, as we include magnetic helicity, we do not expect very different results from those quoted below from previous studies.

In Ref. [20] (see also Ref. [53] for an improved calculation), the authors show that for a PIXIE detectable y-distortion generated after decoupling, i.e. $y \gtrsim 10^{-8}$, a field strength of $B_0 > 0.6$ nG is required for a spectral index of causally generated magnetic fields $n = 2$. As we see in this paper, for magnetic fields generated at the EW scale, a field strength $B_0 \sim$ nG is marginally possible if the field is initially fully helical $f_* \simeq 1$ and the magnetic energy is in equipartition with the photon energy $\varepsilon \simeq 1$ at the time of magnetogenesis [see Fig. 2(b)]. This seems to be a rather unlikely scenario, and hence the contribution to the y-type distortion after decoupling generated from EW scale magnetic fields is probably not detectable. To obtain a field strength of order $B_0 \sim$ nG from fields generated at the QCD scale, a large initial helicity fraction is still required $f_* \gtrsim 10^{-6}$ [see Fig. 3(b)]. Such fields could marginally generate observable y-distortions after decoupling. In this case, the contribution to the y-distortion after decoupling is approximately comparable to the contribution before. In any case, the conclusion remains the same: without significant initial helicity fraction, the magnetic field strengths are too weak in the postdecoupling era to generate PIXIE observable spectral distortions.

Although it is beyond the scope of this current paper, and the main conclusions are not expected to change significantly, it would be interesting to run simulations like those of Refs. [20,53] to investigate the postdecoupling regime while including helical magnetic fields.

IV. CONCLUSIONS

Magnetic fields generated in the very early Universe decay in the radiation dominated epoch due to turbulent MHD effects. The decaying magnetic fields inject energy into the primordial plasma which can lead to μ-type and y-type distortions to the CMB blackbody spectrum. The current COBE/FIRAS limits on these spectral distortions are very tight $|\mu| < 9 \times 10^{-5}$ and $y \lesssim 1.5 \times 10^{-5}$ [14]. However, there is the exciting possibility of a new PIXIE-like experiment which could place much stronger upper limits of $|\mu| < 5 \times 10^{-8}$ and $y \lesssim 10^{-8}$ if no detection is made [47]. Any prediction for spectral distortions above the PIXIE limits is what we call detectable.

In this paper, we consider the evolution of helical and nonhelical magnetic fields generated by some causal process in the early Universe. We calculate the spectral distortions using the decays laws of Refs. [12,13,33]. We find that causally generated nonhelical magnetic fields, with an initial helicity fraction less than $\sim 10^{-14}$, generated at the EW phase transition will not produce any detectable CMB μ-type or y-type spectral distortions. This remains true even if the inverse transfer effect for nonhelical fields seen in Refs. [36,41] is considered. Hence, to produce observable spectral distortions from the decay of magnetic fields generated at the EW phase transition, a non-negligible helical component is required.

Here, we note that, if the inverse transfer effect for nonhelical fields is applicable [36,41], it looks possible to generate small amounts of detectable distortions from magnetic fields generated at the QCD phase transition. We also note that magnetogenesis at the QCD phase transition is disfavored compared to magnetogenesis at the EW phase transition. Under early Universe conditions with very small chemical potentials, the QCD phase transition is a smooth transition [54], whereas the EW phase transition could be first-order in certain Standard Model extensions [55].

The conservation of magnetic helicity in the early Universe leads to an inverse cascade of energy and the slowing down of magnetic decay for fully helical fields. This means that, at the time when CMB spectral distortions can be generated, the magnetic field amplitude is relatively large compared to the nonhelical case. This can lead to the generation of larger spectral distortions. If CMB spectral distortions are observed by some new PIXIE-like experiment, then it is likely that magnetic helicity plays an important role. However, there is a degeneracy in the parameter space, since different parameter sets can give the same spectral distortions signal. For example, fields generated at the QCD phase transition with smaller $\varepsilon \equiv \tilde{\rho}_{B,*}/\rho_{\gamma,0}$ and/or helicity can produce the same μ-type distortions as fields generated at the EW phase transition but with larger ε and/or helicity. We note that mixed-type distortions can break the degeneracies and identify heating mechanisms [25,28]. More generally, if a μ-type distortion is detected by a PIXIE-like experiment, it would rule out nonhelical magnetic fields produced at either the EW or QCD phase transition. A positive detection would give us a lower bound on the primordial magnetic helicity. The lower bound would be somewhere of the order $f_* \gtrsim (10^{-4}–10^{-3})$.

This is much greater than the primordial magnetic helicity generated in the simplest models of EW baryogenesis [56] where $f_* \sim 10^{-24}$ assuming $B_{\lambda,*} = B_{\lambda,*}^{\max}$ and $\lambda_{B,*} = \lambda_{\rm EW}$ [57]. However, there are new mechanisms that have been proposed recently which can excite magnetic helicity in the early Universe due to the Chiral anomaly [58,59]. It will be interesting to investigate such mechanisms in the future.

It is also interesting to mention the recent tentative observations of large scale helical magnetic fields from γ-ray observations [60]. Such studies have seen some evidence, albeit rather weak, of fully helical fields of strength 10^{-14} G on scales of 10 Mpc. If such fields originated from a time before the μ-era, then it is possible that such observations would be accompanied by a detectable signal for a PIXIE-like experiment. The combination of these two observations would be compelling evidence for large scale helical magnetic fields. We also note that the CMB distortions anisotropies (see e.g. Refs. [22,61]), albeit potentially very hard to detect, could give interesting signals due to the large helicity of the magnetic fields. Unique signatures in the spatial correlations are expected due to the helical nature of the magnetic fields. This will be investigated in future publications.

ACKNOWLEDGMENTS

This work was supported by the Deutsche Forschungsgemeinschaft through the collaborative research center SFB 676 Particles, Strings, and the Early Universe, Project No. C9.

[1] R. Beck, Space Sci. Rev. **166**, 215 (2012).
[2] M. L. Bernet, F. Miniati, S. J. Lilly, P. P. Kronberg, and M. Dessauges-Zavadsky, Nature (London) **454**, 302 (2008).
[3] S. Chakraborti, N. Yadav, C. Cardamone, and A. Ray, Astrophys. J. **746**, L6 (2012).
[4] L. Feretti, G. Giovannini, F. Govoni, and M. Murgia, Astrophysics (Engl. Transl.) **20**, 54 (2012).
[5] Y. Xu, P. P. Kronberg, S. Habib, and Q. W. Dufton, Astrophys. J. **637**, 19 (2006).
[6] A. Neronov and I. Vovk, Science **328**, 73 (2010).
[7] M. S. Turner and L. M. Widrow, Phys. Rev. D **37**, 2743 (1988).
[8] G. Sigl, A. V. Olinto, and K. Jedamzik, Phys. Rev. D **55**, 4582 (1997).
[9] E. Harrison, Mon. Not. R. Astron. Soc. **147**, 279 (1970).
[10] A. D. Dolgov and D. Grasso, Phys. Rev. Lett. **88**, 011301 (2001).
[11] M. Christensson, M. Hindmarsh, and A. Brandenburg, Phys. Rev. E **64**, 056405 (2001).
[12] R. Banerjee and K. Jedamzik, Phys. Rev. D **70**, 123003 (2004).
[13] L. Campanelli, Eur. Phys. J. C **74**, 2690 (2014).
[14] D. Fixsen, E. S. Cheng, J. M. Gales, J. C. Mather, R. A. Shafer and E. L. Wright, Astrophys. J. **473**, 576 (1996).
[15] R. A. Sunyaev and Y. B. Zeldovich, Nature (London) **223**, 721 (1969).
[16] W. Hu and J. Silk, Phys. Rev. D **48**, 485 (1993).
[17] R. Khatri, R. A. Sunyaev, and J. Chluba, Astron. Astrophys. **543**, A136 (2012).
[18] J. Chluba, R. Khatri, and R. A. Sunyaev, Mon. Not. R. Astron. Soc. **425**, 1129 (2012).
[19] E. Pajer and M. Zaldarriaga, J. Cosmol. Astropart. Phys. 02 (2013) 036.
[20] K. E. Kunze and E. Komatsu, J. Cosmol. Astropart. Phys. 01 (2014) 009.
[21] K. Jedamzik, V. Katalinic, and A. V. Olinto, Phys. Rev. Lett. **85**, 700 (2000).
[22] K. Miyamoto, T. Sekiguchi, H. Tashiro, and S. Yokoyama, Phys. Rev. D **89**, 063508 (2014).
[23] M. A. Amin and D. Grin, Phys. Rev. D **90**, 083529 (2014).
[24] H. Tashiro, Prog. Theor. Exp. Phys. **2014**, 6B107 (2014).
[25] R. Khatri and R. A. Sunyaev, J. Cosmol. Astropart. Phys. 09 (2012) 016.
[26] W. Hu, D. Scott, and J. Silk, Astrophys. J. **430**, L5 (1994).
[27] P. McDonald, R. J. Scherrer, and T. P. Walker, Phys. Rev. D **63**, 023001 (2000).
[28] J. Chluba and R. A. Sunyaev, Mon. Not. R. Astron. Soc. **419**, 1294 (2012).
[29] J. Chluba, Mon. Not. R. Astron. Soc. **436**, 2232 (2013).
[30] B. J. Carr, K. Kohri, Y. Sendouda, and J. Yokoyama, Phys. Rev. D **81**, 104019 (2010).
[31] H. Tashiro, E. Sabancilar, and T. Vachaspati, J. Cosmol. Astropart. Phys. 08 (2013) 035.
[32] R. Durrer and C. Caprini, J. Cosmol. Astropart. Phys. 11 (2003) 010.
[33] L. Campanelli, Phys. Rev. Lett. **98**, 251302 (2007).
[34] A. Saveliev, K. Jedamzik, and G. Sigl, Phys. Rev. D **86**, 103010 (2012).
[35] A. Saveliev, K. Jedamzik, and G. Sigl, Phys. Rev. D **87**, 123001 (2013).
[36] A. Brandenburg, T. Kahniashvili, and A. G. Tevzadze, Phys. Rev. Lett. **114**, 075001 (2015).
[37] R. Durrer and A. Neronov, Astron. Astrophys. Rev. **21**, 62 (2013).
[38] L. Campanelli, Phys. Rev. Lett. **98**, 251302 (2007).
[39] J. M. Wagstaff, R. Banerjee, D. Schleicher, and G. Sigl, Phys. Rev. D **89**, 103001 (2014).
[40] D. Biskamp, *Cambridge Monographs on Plasma Physics* (Cambridge University Press, Cambridge, England, 1993).
[41] T. Kahniashvili, A. G. Tevzadze, A. Brandenburg, and A. Neronov, Phys. Rev. D **87**, 083007 (2013).
[42] L. Campanelli, Phys. Rev. D **70**, 083009 (2004).
[43] K. Jedamzik and G. M. Fuller, Astrophys. J. **423**, 33 (1994).
[44] P. Ade *et al.* (Planck Collaboration), arXiv:1303.5076.

[45] K. Jedamzik, V. Katalinic, and A. V. Olinto, Phys. Rev. D **57**, 3264 (1998).
[46] P. A. R. Ade *et al.* (Planck Collaboration), arXiv:1502.01589.
[47] A. Kogut *et al.*, J. Cosmol. Astropart. Phys. 07 (2011) 025.
[48] P. A. R. Ade *et al.* (Planck Collaboration), arXiv:1502.01594.
[49] K. E. Kunze and E. Komatsu, J. Cosmol. Astropart. Phys. 06 (2015) 027.
[50] A. Refregier, E. Komatsu, D. N. Spergel, and U.-L. Pen, Phys. Rev. D **61**, 123001 (2000).
[51] S. K. Sethi and K. Subramanian, Mon. Not. R. Astron. Soc. **356**, 778 (2005).
[52] D. R. G. Schleicher, R. Banerjee, and R. S. Klessen, Astrophys. J. **692**, 236 (2009).
[53] J. Chluba, D. Paoletti, F. Finelli, and J.-A. Rubiño-Martín, Mon. Not. R. Astron. Soc. **451**, 2244 (2015).
[54] Y. Aoki, G. Endrodi, Z. Fodor, S. Katz, and K. Szabo, Nature (London) **443**, 675 (2006).
[55] M. Laine and K. Rummukainen, Nucl. Phys. **B535**, 423 (1998).
[56] T. Vachaspati, Phys. Rev. Lett. **87**, 251302 (2001).
[57] J. M. Wagstaff and R. Banerjee, arXiv:1409.4223.
[58] A. Boyarsky, J. Frohlich, and O. Ruchayskiy, Phys. Rev. Lett. **108**, 031301 (2012).
[59] A. Boyarsky, J. Frohlich, and O. Ruchayskiy, arXiv:1504.04854.
[60] H. Tashiro, W. Chen, F. Ferrer, and T. Vachaspati, arXiv:1310.4826.
[61] J. Ganc and M. S. Sloth, J. Cosmol. Astropart. Phys. 08 (2014) 018.